Analyses of Strong Motion Data of the 2006 M 6.7 Kiholo Bay and M 6.0 Mahukona Earthquakes and Ground Motion Prediction Models for Hawaii

FINAL TECHNICAL REPORT

Submitted to the

U.S. Geological Survey
Under the National Earthquake Hazards Reduction Program
Program Element I, National and Regional Earthquake Hazard Assessments

Award No. 08HQGR0036
Period of Performance: 1 January 2008 to 30 June 2010

By

Ivan G. Wong and Mark Dober
URS Corporation, Seismic Hazards Group, 1333 Broadway, Suite 800, Oakland, CA 94612
Phone: (510) 874-3014, E-mail: ivan.wong@urs.com

Walter J. Silva, Robert Darragh, and Nick Gregor
Pacific Engineering & Analysis, 856 Seaview Drive, El Cerrito, CA 94530

26 October 2011

ABSTRACT

In order to assess the level and nature of ground shaking in Hawaii for the purposes of earthquake hazard mitigation and seismic design, empirical ground motion prediction models are desired. However, the models that were used in the Hawaii State hazard maps developed by the U.S. Geological Survey as part of the National Seismic Hazard Map Project have been, with one exception, not specific to Hawaii. In particular, no model, until recently, has been available for the deep Hawaiian events such as the damaging 2006 moment magnitude (**M**) 6.7 Kiholo Bay earthquake that occurred at a depth of 39 km.

The purpose of this study was to develop a ground motion prediction model for deep (> 20 km) Hawaiian earthquakes such as the 2006 earthquake. There was insufficient strong motion data, however, to develop such an empirical model and so we developed a ground motion prediction model based on the stochastic point-source numerical ground motion model. A major input into the stochastic model is stress drop. The 2006 strong motion data and data from 14 other deep Hawaiian earthquakes of **M** 3.3 to 6.2 were inverted using a nonlinear least-squares inversion of Fourier amplitude spectra to estimate stress drops and for the few larger events (**M** ≥ 5.0), to calibrate the stochastic ground motion prediction model. The calculated stress drop for the 2006 earthquake is 97 bars, which may partially explain some of the high recorded ground motions at high frequencies.

The ground motion model is valid for the magnitude range **M** 3.5 to 8.5 over the hypocentral distance range of 20 to 400 km. The model equations are for 5%-damped spectral acceleration at 27 periods from peak horizontal ground acceleration (PGA) to 10.0 sec.

INTRODUCTION

The Island of Hawaii has one of the highest levels of seismic hazard in the U.S. (Klein *et al*., 2001). The 15 October 2006 moment magnitude (**M**) 6.7 Kiholo Bay earthquake, which caused more than $200 million in damage is a recent example of the Big Island's seismic hazard. In order to assess the level and nature of ground shaking in Hawaii for the purposes of earthquake hazard mitigation and seismic design, empirical ground motion prediction models are desired. The models that were used in the Hawaii State hazard maps developed by the U.S. Geological Survey (USGS) as part of the National Seismic Hazard Map Project included (Klein *et al.*, 2001): Munson and Thurber (1997), Boore *et al*. (1997), Sadigh *et al*. (1997), and Campbell

(1997) for the shallow crustal earthquakes (< 20 km depth) and the Youngs *et al*. (1997) intraslab subduction zone model for the deep events (> 20 km). The last relationship was used by default given that no other model was available at the time for the deep Hawaiian events. The relationship by Munson and Thurber (1997) is the only model until recently that has been developed specifically from Hawaiian strong motion data (22 earthquakes, **M** 4.0 to 7.2) but for shallow crustal earthquakes and peak horizontal ground acceleration (PGA) only. The other crustal earthquakes models are appropriate for tectonically active regions such as California.

As mentioned, there was no ground motion prediction model appropriate for deep Hawaiian earthquakes like the 2006 Kiholo Bay event. Atkinson (2010) recently developed a ground motion model for both shallow (depth < 20 km) and deep Hawaiian earthquakes (35 to 40 km) using the Reference Empirical approach and the current database of Hawaiian strong motion records including the 2006 Kiholo Bay earthquake.

The 2006 Kiholo Bay earthquake whose hypocenter was at a depth of 39 km provided the largest suite of strong motion records ever produced for an earthquake in Hawaii and the best opportunity to date to understand the processes of strong ground shaking in the region (Wong *et al*., 2011). The earthquake was recorded on 19 free-field strong motion instruments operated on the Big Island by the USGS and 7 USGS stations on Maui and Oahu (Stephens *et al.*, 2007). PGAs over 1 g were recorded at the North Kohala Police Station (1.12 g) and Waimea Fire Station (1.05 g) (Table 1; Figure 1). Such high PGAs are surprising given the large depth of the earthquake. In addition to the mainshock, a triggered event of **M** 6.0 on the same day occurred at a shallower depth of 19 km near Mahukona and a deep **M** 5.0 aftershock were also recorded by the USGS Hawaiian Strong Motion Network (Figure 1). There were 19 and 13 sets of records of these two events on the Big Island, respectively. The highest recorded PGA for the Mahukona event was 0.26 g (Stephens *et al.*, 2007).

The purpose of this study was to develop a ground motion prediction model for earthquakes of **M** ≥ 5.0 deeper than 20 km beneath the Big Island. The focal depth of 20 km was used in the Hawaii State hazard maps to distinguish between shallow crustal and deep earthquakes in Hawaii (Klein *et al*., 2001). The stochastic numerical ground motion model (Hanks and McGuire, 1981; Boore, 1983; Silva *et al.*, 1997) was used to develop the ground motion prediction model similar to what we have done in several regions in the western U.S. (Gregor *et al.*, 2002; Wong *et al.*,

2002; 2004; 2005) and central and eastern U.S. (e.g., Silva *et al.*, 2002; 2003). We used the 2006 strong motion data and data from other deep events to invert for stress drop, an important input into the stochastic model and for the few larger events (**M** ≥ 5.0), to calibrate the ground motion prediction model.

DEEP EARTHQUAKES

The island of Hawaii is one of the most seismically active regions in the U.S., with seismicity and seismic hazard on par with coastal California, although it is far from a tectonic plate boundary. Most of this seismicity is at least indirectly related to volcanism, explaining why 43 **M** > 6 earthquakes have occurred on the volcanically active Big Island since 1868, whereas only 8 such events have occurred in the rest of the Hawaiian Island chain (Klein *et al*., 2001).

Earthquakes in Hawaii fall into several categories. Most are concentrated under the active volcanoes of Mauna Loa, Kilauea, and Hualalai and are related to the migration and intrusion of magma under and into the volcanoes. Small earthquakes caused by migration of magma often occur in shallow swarms, especially preceding an eruption. In addition, many of Hawaii's largest earthquakes are related to magma injection along major rift zones that flank the active volcanoes. These earthquakes are triggered when the seaward block flanking the rift zone slips laterally on a subhorizontal décollement away from the rift as it makes way for intruding magma and relieves the stored stress (Klein *et al*., 2001; EERI, 2006). Two of Hawaii's largest historical earthquakes, the 1868 **M** 7.9 Kau district earthquake and the 1975 **M** 7.2 Kalapana earthquake, occurred as a result of such décollement slip (Wyss, 1988; Stover and Coffman, 1993).

Another category of earthquake in Hawaii is indirectly related to volcanism and includes earthquakes that occur primarily in the upper mantle, i.e., 20 to 60 km deep. These earthquakes tend to occur in a ring surrounding the island and are probably caused by fracturing in response to lithospheric flexure under the weight of the overlying volcanic edifice (EERI, 2006; Kirby and Klein, 2006). Earthquakes of this type include the 1868 **M** ~6.5 west Island, 1927 **M** ~6.8 offshore Mauna Kea, 1938 **M** 7 Maui, the 1973 **M** 6.2 Honomu, and the 2006 **M** 6.7 Kiholo Bay earthquakes (Klein *et al.*, 2001).

The 2006 **M** 6.7 Kiholo Bay earthquake was situated towards the western end of the Hualalai rift zone (Figure 1). It occurred on a N14°W-striking fault dipping 76° down to the east (Johnston *et al*., 2007).

STRONG GROUND MOTION DATA

A total of 19 sets of three-component strong motion records from the Big Island were collected and processed by the USGS for the 2006 Kiholo Bay earthquake (Stephens *et al.*, 2007). As an example, the Waimea Fire Station recordings are shown on Figure 2. Other recordings of deep events principally from the USGS database are listed on Table 2. The data for the 1973 earthquake was provided to us by Gail Atkinson. Only a few events had assigned **M** values and so the coda duration (M_C) and Richter local (M_L) magnitudes were assumed to be equivalent to **M**. Events ranged from **M** 3.3 to 6.7 (Table 2). Although there are an insufficient number of recordings, particularly at **M** ≥ 5.0 (only 3 events; Table 2), to develop an empirical model for deep Hawaiian earthquakes based on a regression of the data, the data was used in an inversion for selected point source, path, and site parameters and to calibrate the stochastic relationships.

INVERSIONS FOR STRESS DROPS

A key parameter needed in the stochastic point-source model is stress drop (also called stress parameter). In previous stochastic point-source models, the distribution of stress drops has relied on the observed values for crustal earthquakes. For example, based on inversions of the Next Generation of Attenuation (NGA) ground motion models, median magnitude-dependent stress drops have been estimated by the second author: **M** 4.5 and 5.5, 64 bars; **M** 6.5, 22 bars; and **M** 7.5 and 8.5, 7 bars. The issue for the deep Hawaiian earthquakes is what are their stress drops? Given their volcanic origin, a difference with western U.S. crustal earthquakes would not be surprising.

The approach utilized in this study uses an inversion scheme developed by the second author. In the inversion scheme, earthquake point-source, path and site parameters are obtained by using a Levenberg-Marquardt nonlinear least-squares inversion of Fourier amplitude spectra. The point-source parameters are those that are incorporated into the stochastic ground motion model. The usable bandwidth for each amplitude spectrum computed from the strong motion recordings are selected based upon examination of the Fourier amplitude spectrum at high and low frequencies.

The inversion scheme treats multiple earthquakes and sites simultaneously with the common crustal path damping parameter Q(f). The parameter covariance matrix is examined to determine which parameters may be resolved for each data set. Asymptotic standard errors are computed at the final iteration. The five parameters which may be determined include: kappa, Q_0, and η (frequency-dependent path Q model), **M**, and corner frequency. Crustal and soil profile amplification is accommodated in the inversion scheme by incorporating the appropriate mean amplification functions in the model spectra.

The stress drop is calculated from the moment and corner frequency using the relation for a circular fault model (Brune, 1970; 1971):

$$f_C = \beta_0 \left(\frac{\Delta\sigma}{8.44 \cdot M_0}\right)^{\frac{1}{3}} \qquad (1)$$

To reduce the non-uniqueness inherent in inversion schemes, a suite of starting models is employed. The final set of parameters is selected based upon a visual inspection of the model fit to the Fourier amplitude spectrum, the chi-square values, and the parameter covariance matrix. In the inversions, **M** was fixed at the values shown in Table 2.

The inversions are done on log-amplitude spectra since strong ground motion data appear to be log-normally distributed. This is consistent with the model being represented as a product (rather than sum) of models. The inversion bandwidth is magnitude-dependent, extending to longer periods with increasing magnitudes. The low-frequency limit is site-dependent and may be seen in the Fourier amplitude spectra (model and data). A high-frequency limit was set at 20 Hz (noise contamination permitting) to reduce the tendency toward high-frequency weighting when using linear-frequency spacing. Tests were performed using spectra smoothed over a constant log-frequency window to provide exactly equal weighting. However, this procedure results in poorer fits (for fixed **M**) possibly due to the models' tendency to overpredict low-frequency amplitudes at close distances. In keeping with the model's simplicity, the point-source distance metric uses hypocentral distance for the inversions.

The geometrical spreading factor is fixed in the inversions as R^{-1} at or within RO and $R^{-1/2}$ beyond RO with RO determined in the inversion. RO is the distance where it is assumed there is a change from a body-wave rate to a surface wave rate. The inversion code permits multiple stations treated

as the same site. Distinct kappa values are determined for each site and multiple stations (at varying distances) may be specified as belonging to a single site (or category). Starting stress drops and kappa models were taken as 50 bars and 0.04 sec, respectively, typical values for the western U.S.

A near-surface V_S model was developed by computing a mean profile of the V_S profiles beneath the stations of the USGS Hawaiian Strong Motion Network on the Big Island (Figure 3). The V_S profiles were measured beneath each station based on Spectral-Analysis-of-Surface-Waves (SASW) surveys (Wong *et al.*, 2011). All the stations are underlain by soil, weathered and unweathered basalt (Table 3). V_S30 (average shear-wave velocity in the top 30 m) ranges from 437 to 1,902 ft/sec (133 to 580 m/sec).

Based on the mean V_S profile, a generic shallow soft rock profile was developed and placed on top of a regional crustal model (Figure 3). The V_S30 of the generic profile is 1,404 ft/sec (428 m/sec) reflecting very firm soil but with a steep velocity gradient reaching over 2,000 ft/sec (610 m/sec) at a depth of 100 ft (30.5 m) and about 3,000 ft/sec (914 m/sec) at about 500 ft (152 m).

For the regional crustal model, the P-wave (V_P) and V_S model used by the Hawaiian Volcano Observatory (HVO) in their earthquake locations was adopted (Table 4). The V_S model is based on the V_P model assuming a V_P/V_S ratio of 1.78.

The results of the inversions for stress drops are plotted versus **M** on Figure 4. The stress drops range from 16 bars to more than 800 bars, over an order of magnitude. There is no apparent dependence on magnitude, although the sample size is too small for definitive conclusions. The mean stress drop is 113 bars. This value is higher than typical stress drops for western U.S. earthquakes. The computed stress drop for the 2006 mainshock is 97 bars, which may partially explain the high PGAs recorded at some of the strong motion stations.

The mean to median stress drop ratio, based on the logarithmic fit to the Fourier amplitude spectrum was 1.48. To provide stress drops for the point-source simulations, which uses random vibration theory (RVT) and which requires a mean power spectrum, the 113 bar stress drop was scaled to 167 bars using the mean to median ratio (rounded to 170 bars for the simulations; Table 5). A mean kappa of 0.0245 sec results from the inversions.

STOCHASTIC MODELING AND INPUTS

In this study, the point-source model (Silva *et al.*, 1997) was used to model earthquakes of **M** 3.5, 4.5, 5.5, 6.5, 7.5, and 8.5 in the hypocentral distance range of 20 to 400 km.

Point-Source Parameters

A magnitude-independent mean stress drop of 170 bars based on the inversions was input into the stochastic modeling with low and high range values of 62.4 and 462.1 bars, respectively (Table 5). The σ_{ln} of 0.50 was adopted from the analyses by Silva *et al*. (1997) where 16 earthquakes of **M** 5.3 to 7.4 were modeled at 503 sites to estimate the model bias of the stochastic model and variability. A mean focal depth of 33 km was also used in the modeling but it was randomly varied with a σ_{ln} of 0.26 with bounds of 20 and 50 km (Table 5).

Crustal Model and Attenuation

The crustal model used in the inversions was also input into the stochastic modeling. A frequency-dependent Q(f) relationship of the form:

$$Q\ f\ = Q_O\ \frac{[1+(f/f_Q)]^{\alpha_1}}{(\frac{f}{f_Q})^{\alpha_2}} \qquad (2)$$

was used (Boore, 1984) with $Q_o = 50$, $f_Q = 0.2$, $\alpha_1 = 0.6$, and $\alpha_2 = 1.2$. To stabilize the inversions α_1, α_2, and f_Q were fixed at a suite of values with the final model based on the smallest residuals and Q_o determined by the inversions.

Site Model

The site model used in the inversions was also used in the stochastic modeling. A feature of our model compared to Atkinson (2010) is the use of the V_S profiles beneath the USGS strong motion stations on the Big Island (Table 3; Wong *et al.*, 2011). Atkinson (2010) developed her model prior to the availability of the V_S30 database but noted that the impact would be a 10 to 15% higher bias in her model. Atkinson (2010) has incorporated V_S30 into her ground motion model in contrast to this study where we are assuming average basalt site conditions on the Big Island.

The kappa of 0.0245 sec from the inversions was input into the stochastic modeling (Table 5). The standard error of σ_{ln} 0.30 is derived from Silva *et al*. (1997).

RESULTS

To accommodate finite-source effects at large magnitude, model simulations included an empirical magnitude-dependent short-period saturation as well as a magnitude-dependent, far-field fall-off (Silva *et al*., 1997). These effects are accommodated by adding a magnitude-dependent term to the source depth as well as a magnitude-dependent geometrical attenuation. Coefficients for the two models are based on the Abrahamson and Silva (1997) empirical ground motion model for the western U.S. (Silva *et al*., 1997). Both the magnitude saturation and magnitude-dependent far-field fall-off are similar to the empirical trends exhibited in the Abrahamson and Silva (1997) model.

Aleatory variabilities in stress drop, point-source depths, the crustal attenuation parameters Q_o and η, and kappa were included in the computations of the model through parametric variations (Table 5).

Variability (aleatory) in the regression of the simulated data is added to the modeling variability (Silva *et al.*, 1997) to produce 16th, 50th (median), and 84th percentile relationships. A total of 30 simulations was made for each magnitude and distance (total of 1,620 sets of calculations), and the results fitted with a functional form that accommodates magnitude-dependent saturation as well as far-field fall-off. The functional form is:

$$\text{Ln } Y = C_1 + C_2 \bullet \mathbf{M} + (C_4 + C_5 \bullet \mathbf{M}) \bullet \text{Ln}[R + \exp(C_3)] + C_6 (\mathbf{M}\text{-}6)^2 \qquad (3)$$

where Y is the median (average horizontal component) ground motion parameters, R is Joyner-Boore (JB) distance, and C_1 through C_6 are coefficients fit to the data (Table 6). Ground motions were calculated for a total of 27 periods from PGA to 10.0 sec. The total aleatory variability (vector sum of the parametric and modeling variability) is also listed in Table 6.

To provide a quantitative measure of the uncertainties in the ground-motion predictions, a simple goodness-of-fit was performed at each spectral period. The modeling uncertainty is the average at each frequency of the difference of the natural logarithms of the observed ground motions and the model-predicted ground motions.

Figure 5 shows the parametric, modeling, and total sigmas for the stochastic ground motion prediction model. Modeling sigma is based on the modeling misfit at the 503 sites for 16 earthquakes recorded in tectonically active areas (Silva *et al*., 1997). Because the sharp increase in model variability at periods beyond about 2 sec is largely due to data limitations at long period, it is recommended the variability at 2 sec be used for longer periods.

COMPARISONS

Our model is appropriate for average basalt site conditions. Figures 6 to 8 compare our model for a **M** 6.7 earthquake at a depth of 38.9 km and basalt site conditions with the recorded PGA and 0.2 and 1.0 sec SA values from the 2006 Kiholo Bay earthquake. The 2006 ground motions are plotted as a function of NEHRP site class as determined by Wong *et al.* (2011). The site class is unknown for a few strong motion sites, which are located on the other islands. Also shown is the ground motion model of Atkinson (2010). For her model, we use the V_S30 of 428 m/sec. Median and ± sigma curves are shown for both models.

For the 2006 PGAs, which range over an order of magnitude, the ± one sigma curves in our model captures much of the data although it clearly underpredicts the values for several stations (Figure 6). The larger aleatory uncertainty in the Atkinson (2010) captures the range in the 2006 PGAs better than our model. Note the significant difference in the fall-off of the two models beyond 100 km (Figure 6). In general, our model falls off faster than the Atkinson (2010) model. The station recordings on the other islands suggest a rapid fall-off.

For 0.2 sec spectral acceleration (SA), our model trends through the center of the large range of observed values as does the Atkinson (2010) model (Figure 7). Finally, at 1.0 sec SA, both models significantly overestimate the data (Figure 8).

Atkinson (2010) observed that her results for 35 to 40 km-deep earthquakes indicated that the ground motion amplitudes at high frequencies were higher than shallow crustal earthquakes as exemplified in the Boore and Atkinson (2008) NGA model.

In Figures 9 to 14, we compare our model and the Atkinson (2010) model with the only other two other deep earthquakes of **M** 5.0 and larger, which have strong motion data (see Table 2): the 17 July 2005 **M** 5.1 and the 23 November 2006 **M** 5.0 aftershock of Kiholo Bay. We plot the ground motions separately because the two events have very different ranges in spectral

accelerations. Our model tends to overpredict slightly the ground motions for the **M** 5.1 event, similar to the Atkinson (2010) model (Figures 9 to 11). For the **M** 5.1 earthquake, both models do a reasonable job of matching the strong motion data (Figures 12 to 14).

In comparison with the Atkinson (2010) model, our model predicts lower ground motions particularly at small magnitudes and at long periods, e.g., 1.0 sec SA.

CONCLUSIONS

In this study, we have developed a ground motion prediction model for deep (> 20 km) earthquakes beneath the Island of Hawaii based on the stochastic ground motion model calibrated with the available strong motion database of deep events. Stress drop is an important input parameter for the stochastic model and we have inverted the available strong motion records for this parameter arriving at a mean value of 113 bars higher than what is typically observed in the western U.S. The computed stress drop for the 2006 Kiholo Bay earthquake is 97 bars. For a future **M** 7.0 earthquake at the shallowest depth of 20 km that our model is valid, it predicts a median PGA of 0.48 g, which would be a damaging level of ground motions. The ± one sigma values are 1.05 and 0.22 g, respectively.

ACKNOWLEDGMENTS

Our thanks to Melinda Lee, Fabia Terra, and Judith Zachariasen for their assistance in the preparation of this paper. Our thanks to Gail Atkinson for providing us processed strong motion data. Information on the North Kohala Police Station record was provided to us by Chris Stephenson. This work was supported by the USGS, Department of Interior, under a NEHRP grant award 08HQGR0036. The views and conclusions contained in this document are those of the authors and should not be interpreted as necessarily representing the official policies, either expressed or implied of the U.S. Government.

REFERENCES

Atkinson, G.M., 2010, Ground motion prediction equations for Hawaii from a referenced empirical approach: Bulletin of the Seismological Society of America, v. 100, p. 751-761.

Boore, D.M., 1983, Stochastic simulation of high-frequency ground motions based on seismological models of the radiated spectra: Bulletin of the Seismological Society of America, v. 73, p. 1865-1984.

Boore, D.M., 1984, Use of seismoscope records to determine M_L and peak velocities: Bulletin of the Seismological Society of America, v. 74, p. 315-324.

Boore, D.M., Joyner, W.B., and Fumal, T.E., 1997, Equations for estimating horizontal response spectra and peak acceleration from western North American earthquakes: A summary of recent work: Seismological Research Letters, v. 68, p. 128-153.

Brune, J.N., 1970, Tectonic stress and the spectra of seismic shear waves from earthquakes: Journal of Geophysical Research, v. 75, p. 4997-5009.

Brune, J.N., 1971, Correction: Journal of Geophysical Research, v. 76, p. 5002.

Campbell, K.W., 1997, Empirical near-source attenuation relationships for horizontal and vertical components of peak ground acceleration, peak ground velocity, and pseudo-absolute acceleration response spectra: Seismological Research Letters, v. 68, p. 154-179.

EERI (Earthquake Engineering Research Institute), 2006, Preliminary observations on the Hawai'i earthquakes of October 15, 2006, EERI Special Earthquake Report, insert to EERI Newsletter, December 2006, v. 40, 8 pp.

Gregor, N., Silva, W., Wong, I., and Youngs, R., 2002, Ground motion attenuation relationships for Cascadia subduction zone megathrust earthquakes based on a stochastic finite-fault model, Bulletin of the Seismological Society of America, v. 92, p. 1923-1932.

Hanks, T.C. and McGuire, R.K., 1981, The character of high-frequency strong ground motion Bulletin of the Seismological Society of America, v. 71, p. 2071-2095.

Johnston, M.J.S., Lisowski, M., and Linde, A.T., 2007, Response of Mauna Loa volcano to the October 15, 2006 M 6.7 Kiholo Bay, Hawaii, earthquake: Seismological Research Letters, v. 78, p. 296.

Kirby, S.H. and Klein, F.W., 2006, The 15 October 2006-to-present earthquakes beneath the island of Hawaii: implications for Pacific plate flexure and geomechanical effects of ascending CO2 that embrittles the Pacific plate mantle, Eos Trans. AGU, 87(52), Fall Meet. Suppl., Abstract 253E-07.

Klein, F.W., Frankel, A.D., Mueller, C.S., Wesson, R.L., and Okubo, P.G., 2001, Seismic hazard in Hawaii: high rate of large earthquakes and probabilistic ground-motion maps: Bulletin of the Seismological Society of America, v. 91, p. 479-498.

Munson, C.G. and Thurber, C.H., 1997, Analysis of the attenuation of strong ground motion on the island of Hawaii: Bulletin of the Seismological Society of America, v. 87, p. 945-960.

Sadigh, K., Chang, C.Y., Egan, J.A., Makdisi, F., and Youngs, R.R., 1997, Attenuation relationships for shallow crustal earthquakes based on California strong motion data: Seismological Research Letters, v. 68, p. 180-189.

Silva, W.J., Abrahamson, N.A., Toro, G., and Constantino, C., 1997, Description and validation of the stochastic ground motion model, unpublished report prepared for the Brookhaven National Laboratory.

Silva, W., Gregor, N., and Darragh, R., 2002, Development of regional hard rock attenuation relations for central and eastern North America, unpublished report prepared by Pacific Engineering and Analysis (available on the PE&A website).

Silva, W., Wong, I., Siegel, T., Gregor, N., Darragh, R., and Lee, R., 2003, Ground motion and liquefaction simulation of the 1886 Charleston, South Carolina, earthquake: Bulletin of the Seismological Society of America, v. 93, p. 2717-2736.

Stephens, C.D., Savage, W.U., Okubo, P.G., and Anjal, E.C., 2007, Update on strong-motion recordings of the October 15, 2006, M 6.7 Kiholo Bay, HI, earthquake sequence, Seismological Reach Letters, v. 78, p. 303.

Stover, C.W. and Coffman, J.L., 1993, Seismicity of the United States, 1568-1989 (Revised), U.S. Geological Survey Professional Paper 1527, United States Government Printing Office, Washington, 427 pp.

Wong, I., Olig, S., Dober, M., Silva, W., Wright, D., Thomas, P., Gregor, N., Sanford, A., Lin, K-W., and Love, D., 2004, Earthquake scenario and probabilistic ground shaking hazard maps for the Albuquerque-Belen-Santa Fe, New Mexico corridor, New Mexico Geology**,** v. 26, p. 1-35.

Wong, I., Olig, S., Dober, M., Wright, D., Nemser, E., Lageson, D., Silva, W., Stickney, M., Lemieux, M., and Anderson, L., 2005, Probabilistic earthquake hazard maps for the State of Montana, Montana Bureau of Mines and Geology Special Publication 117, 73 p. with CD-ROM.

Wong, I., Silva, W., Olig, S., Thomas, P., Wright, D., Ashland, F., Gregor, N., Pechmann, J., Dober, M., Christenson, G., and Gerth, R., 2002, Earthquake scenario and probabilistic ground shaking maps for the Salt Lake City, Utah, metropolitan area: Utah Geological Survey Miscellaneous Publication MP-02-05.

Wong, I.G., Silva, W.J., Youngs, R.R., Stark, C.L., 1996, Numerical earthquake ground motion modeling and its use in microzonation: Proceedings of the 11th World Conference on Earthquake Engineering, Pergamon (CD-ROM).

Wong, I, Stokoe, K., Cox, B., Yuan, J., Knudsen, K., Terra, F., Okubo, P., and Lin, C-Y., 2011, Shear-wave velocity characterization of the USGS Hawaiian strong motion network on the Island of Hawaii and development of a NEHRP site class map, Bulletin of the Seismological Society of America, v. 101, p. 2252-2269.

Wyss, M., 1988, A proposed source model for the great Kau, Hawaii, earthquake of 1868, Bulletin of the Seismological Society of America, v. 78, p. 1450-1462.

Youngs, R.R., Chiou, S.-J, Silva, W.J., and Humphrey, J.R., 1997, Strong ground motion attenuation relationships for subduction zone earthquakes: Seismological Research Letters, v. 68, p. 58-73.

Table 1. PGA Values Recorded in the 2006 Kiholo Bay Earthquake

Station Name	Hypocentral Distance to Mainshock (km)	M 6.7 (g's)
Waikoloa Marriott Hotel, Anaehoomalu	39.5	0.19
Kailua-Kona Fire Station	46.9	0.27
Waimea Fire Station	50.9	1.05
Kona Community Hospital, Kea Lakekua	55.4	0.52
North Kohala Police Station, Kapaau	56.8	1.12
Mauna Kea State Park	59.2	0.32
Mauna Kea Summit	62.4	0.26
Honaunau Post Office	64.4	0.20
Mauna Loa Weather Observatory	66.0	0.23
Honokaa Police Station	66.7	0.65
Laupahoehoe Post Office	84.0	0.36
Hawaiian Volcano Observatory	93.2	0.06
Hilo Medical Center	95.9	0.08
USDA Laboratory, Hilo	97.4	0.24
Ka`u Hospital, Pahala	97.5	0.18
University of Hawaii, Hilo	99.5	0.06
Mountain View Post Office	101.7	0.07
Ka`u Baseyard, Waiohinu	103.2	0.13
Pahoa Fire Station	118.6	0.08

Note: Mainshock not recorded at Mac Farms (Honomalino), South Kohala Fire Station (Kamuela), and NWS Data Regional Center (Hilo).

Table 2. List of Hawaiian Strong Motion Data for Deep (> 20 km) Earthquakes

Earthquake	Date/Time (UTC)	Magnitude	Type	Depth (km)	Latitude (degrees)	Longitude (degrees)	No. of Stations
Honomu	26 Apr 1973 20:26	6.2	**M**	38.7	19.865	-155.153	2
Kailua	13 Dec 2002 03:16	3.7	M_C	24.7	19.636	-155.849	3
Offshore Kailua	15 Dec 2002 05:31	3.5	M_C	45.1	19.643	-156.175	3
Volcano	25 Jan 2003 16:46	3.9	M_L	29.3	19.372	-155.327	8
Mauna Kea Summit	10 Jul 2003 15:59	3.4	M_C	26.3	19.823	-155.366	3
Kailua	18 Sep 2003 06:34	3.4	M_C	45.4	19.771	-156.085	1
Kilauea	11 Oct 2004 20:29	4.0	M_C	31.8	19.346	-155.276	2
Waikii	13 Jan 2005 06:16	3.6	M_C	20.1	19.938	-155.546	2
S. Hawaii Island	17 Jul 2005 19:15	5.1	**M**	28.4	18.809	-155.446	14
Pohakuloa	22 Nov 2005 19:57	3.3	M_C	22.6	19.825	155.575	1
Naalehu	19 Jan 2006 02:04	4.3	**M**	40.0	19.053	-155.430	5
Kiholo Bay	15 Oct 2006 17:07	6.7	**M**	38.9	19.878	-155.935	23
Waikoloa	13 Nov 2006 01:36	3.7	M_C	36.2	19.899	-155.848	13
Puako	23 Nov 2006 19:20	5.0	**M**	37.7	19.890	-155.979	13
Hakalau	03 Jul 2007 22:28	3.8	M_C	40.2	19.911	-155.123	11

M_L = Richter local magnitude
M_C = Coda duration magnitude
M = Moment magnitude

Table 3. Site Characteristics of the Island of Hawaii Strong Motion Stations (from Wong *et al*., 2011)

Station No.	Station Location	Longitude (degrees)	Latitude (degrees)	Maximum Profile Depth (ft)	V_S30 (ft/sec)	NEHRP Site Class	Geotechnical Layering Profiles Based on V_S
2810	Kailua-Kona Fire Station	-155.9923	19.6477	100	1418	C	13 ft soil▲/43 ft weathered basalt▼/basalt○
2812	Ka'u Hospital, Pāhala	-155.4723	19.1999	286	1389	C	1.5 ft soil/284+ ft weathered basalt
2816	Pahoa Fire Station	-154.9466	19.4934	120	1497	C	10 ft soil/40 ft weathered basalt/basalt
2817	University of Hawaii, Hilo	-155.0805	19.7034	144	1615	C	1.5 ft soil/42.5 ft weathered basalt/basalt
2818	USDA Laboratory, Hilo	-155.0974	19.7277	116	437	E	70+ ft very soft soil/46+ ft soft soil
2822	Ka'u Baseyard, Waiohinu	-155.6150	19.0700	124	1365	C	1.5 ft soil/120+ ft weathered basalt
2824	Mauna Loa Weather Observatory	-155.5770	19.5363	318	1120	D	140 ft soil/130 ft weathered basalt/basalt
2825	Waimea Fire Station	-155.6614	20.0230	100	1375	C	16 ft soil/29 ft weathered basalt/basalt
2826	North Kohala Police Station	-155.8010	20.2300	198	1006	D	80 ft soil/60 ft weathered basalt/basalt
2829	Mauna Kea State Park	-155.5300	19.7520	192	1150	D	100 ft soil/30 ft weathered basalt/basalt
2830	Mauna Kea Summit	-155.4730	19.8260	156	1149	D	80 ft soil/basalt
2832	Honokaa Police Station	-155.4625	20.0775	154	1205	C	24 ft soil/66 ft weathered basalt/basalt
2833	Laupahoehoe Post Office	-155.2326	19.9835	172	1005	D	50 ft soil/122+ ft weathered basalt
2834	Mac Farms, Honomalino	-155.8680	19.1690	189	1086	D	120 ft soil/basalt
2836	Hawaiian Volcano Observatory	-155.2880	19.4200	156	890	D	130 ft soft soil/26+ ft soil
2839	Hilo Medical Center	-155.1150	19.7220	202	1430	C	15 ft soil/80 ft weathered basalt/basalt
2845	Honaunau Post Office	-155.8805	19.4174	100	1559	C	100+ ft weathered basalt
2846	Mountain View Post Office	-155.1083	19.5504	123	1159	D	35 ft soil/88+ ft weathered basalt
2847	Waikoloa Marriott Hotel, Anaehoomalu	-155.8870	19.9190	150	1550	C	26 ft soil/basalt
2849	Kona Community Hospital, Kea Lakekua	-155.9181	19.5215	200	1476	C	8 ft soil/78 ft weathered basalt/basalt
2852	South Kohala Fire Station, Kamuela	-155.8343	19.9464	266	1902	C	3.5 ft soil/50.5 ft weathered basalt/basalt
2853	NWS Data Regional Center, Hilo	-155.0460	19.7154	203	1176	D	203+ ft soil

▲ Soil refers to stiff soil category
▼ Weathered basalt refers to material category
○ Basalt refers to material category
+ Minimum thickness

NEHRP Site Class V_S30

A > 5,000 ft/sec
B 2,500 to 5,000 ft/sec
C 1,200 to 2,500 ft/sec
D 600 to 1,200 ft/sec
E < 600 ft/sec

Table 4. Crustal V_P and V_S Model for the Island of Hawaii

Depth* (km)	V_P (km/sec)	V_S (km/sec)
0.0	2.2	1.2
0.5	2.7	1.5
1.0	3.2	1.8
1.5	3.7	2.1
2.0	4.2	2.4
2.5	4.7	2.6
3.0	5.2	2.9
3.5	5.7	3.2
4.0	6.2	3.5
4.5	6.5	3.7
7.0	6.8	3.8
15.0	7.2	4.0
15.5	7.6	4.3
16.0	8.0	4.5
16.5	8.1	4.6

* Depth to top of layer

Table 5. Point-Source and Path Input Parameters and Standard Errors Used in the Development of the Stochastic Ground Motion Prediction Model

Parameter	Values	Standard Errors σ_{ln}
Magnitude (**M**)	3.5, 4.5, 5.5, 6.5, 7.5, 8.5	—
Distance (km)	1, 5, 10, 20, 50, 75, 100, 200, 400	
Point-Source Depth (km)[1]	33 km	0.26
Stress Drop (bars)[1]	170	0.50[2]
Crustal Attenuation[1]		
Q_O	50	0.40[2]
f_Q	0.2	—
α_1	0.6	—
α_2	1.2	—
Kappa (sec)	0.0245	0.30[2]
Crustal Model	See Table 4	—

[1] Parameters randomly varied where σ_{ln} is based on observations
[2] From Silva *et al*. (1997)

Table 6. Coefficients and Standard Errors

Frequency (Hz)	C_1	C_2	C_3	C_4	C_5	C_6	Parametric Sigma	Model Sigma	Total Sigma
PGA	68.52187	-5.09631	5.80000	-12.96010	1.03629	-.14898	.6172	.4774	.7803
.100	-6.91550	1.66675	5.40000	-3.03522	.18615	-.15158	.2945	1.2756	1.3092
.200	-.08881	1.63345	5.70000	-3.56561	.15429	-.23807	.3392	1.1358	1.1854
.331	9.41267	1.23611	5.90000	-4.64883	.18193	-.28698	.3861	.9702	1.0442
.501	21.84053	.61910	6.10000	-6.22484	.24654	-.30737	.3986	.8636	.9512
.631	25.11810	.51244	6.10000	-6.58828	.24816	-.31414	.4100	.7680	.8706
1.000	32.93593	.08357	6.10000	-7.51731	.28394	-.31387	.4398	.6627	.7954
1.349	43.47321	-.50426	6.20000	-8.89132	.35245	-.30295	.4883	.6566	.8183
1.995	46.91267	-.93125	6.10000	-9.36813	.40094	-.27491	.5676	.5902	.8188
2.512	58.53881	-1.71001	6.20000	-10.95674	.50386	-.25817	.6228	.5655	.8412
3.311	73.99161	-2.90241	6.30000	-13.06945	.66484	-.23860	.6400	.5581	.8492
4.169	91.64108	-4.50724	6.40000	-15.47178	.88528	-.22629	.6315	.5330	.8264
5.012	98.22293	-5.32783	6.40000	-16.41981	1.00088	-.20822	.6565	.5209	.8381
6.310	106.93830	-6.37317	6.40000	-17.69223	1.15058	-.19072	.6497	.5103	.8261
6.607	108.81360	-6.61834	6.40000	-17.96824	1.18618	-.18760	.6526	.5113	.8290
8.318	106.72080	-7.05038	6.30000	-17.84235	1.26035	-.17244	.6654	.5184	.8435
10.000	103.04320	-7.20814	6.20000	-17.48802	1.29736	-.16376	.6569	.4997	.8254
12.589	109.74360	-8.23258	6.20000	-18.51599	1.45171	-.14918	.6755	.4866	.8325
14.454	102.11800	-7.86625	6.10000	-17.56159	1.41182	-.14031	.6823	.4887	.8393
16.596	93.82941	-7.33934	6.00000	-16.49267	1.34782	-.13461	.6789	.4918	.8383
18.197	85.58938	-6.72014	5.90000	-15.38958	1.26654	-.13275	.6781	.4852	.8338
19.953	85.62312	-6.76578	5.90000	-15.41352	1.27568	-.13241	.6740	.4890	.8327
25.119	78.01486	-6.22686	5.80000	-14.39446	1.20623	-.12877	.6714	.4846	.8280
30.903	69.46166	-5.48027	5.70000	-13.19430	1.10188	-.13149	.6646	.4793	.8194
39.811	67.40193	-5.24299	5.70000	-12.88585	1.06672	-.13721	.6520	.4744	.8063
50.119	65.29077	-4.98649	5.70000	-12.56134	1.02752	-.14202	.6393	.4768	.7975
100.000	68.77858	-5.13883	5.80000	-13.00533	1.04366	-.14918	.6189	.4774	.7816
PGV	39.70192	-2.85255	5.30000	-8.55941	.80414	-.15077	.4487		

List of Figure Captions

Figure 1. USGS strong motion stations and recorded PGA's from the 2006 mainshock.

Figure 2. 2006 Kiholo Bay earthquake acceleration time histories from the Waimea Fire Station. Hypocentral distance was 51 km.

Figure 3. Shallow generic V_S profile used in inversions and stochastic modeling. The V_S30 of the profile is 428 m/sec.

Figure 4. Stress drop versus **M** results from inversions.

Figure 5. Parametric, modeling, and total sigmas.

Figure 6. Comparison of predicted PGA values from the Atkinson (2010) model and this study's model for deep Hawaiian earthquakes and the recorded 2006 mainshock values.

Figure 7. Comparison of predicted 0.2 sec SA values from the Atkinson (2010) model and this study's model for deep Hawaiian earthquakes and the recorded 2006 mainshock values.

Figure 8. Comparison of predicted 1.0 sec SA values from the Atkinson (2010) model and this study's model for deep Hawaiian earthquakes and the recorded 2006 mainshock values.

Figure 9. Comparison of predicted PGA values from the Atkinson (2010) model and this study's model and the recorded 17 July 2005 **M** 5.1 earthquake values.

Figure 10. Comparison of predicted 0.2 sec SA values from the Atkinson (2010) model and this study's model and the recorded 17 July 2005 **M** 5.1 earthquake values.

Figure 11. Comparison of predicted 1.0 sec SA values from the Atkinson (2010) model and this study's model and the recorded 17 July 2005 **M** 5.1 earthquake values.

Figure 12. Comparison of predicted PGA values from the Atkinson (2010) model and this study's model and the recorded 2006 **M** 5.0 Puako aftershock values.

Figure 13. Comparison of predicted 0.2 sec SA values from the Atkinson (2010) model and this study's model and the recorded 2006 **M** 5.0 Puako aftershock values.

Figure 14. Comparison of predicted 1.0 sec SA values from the Atkinson (2010) model and this study's model and the recorded 2006 **M** 5.0 Puako aftershock values.

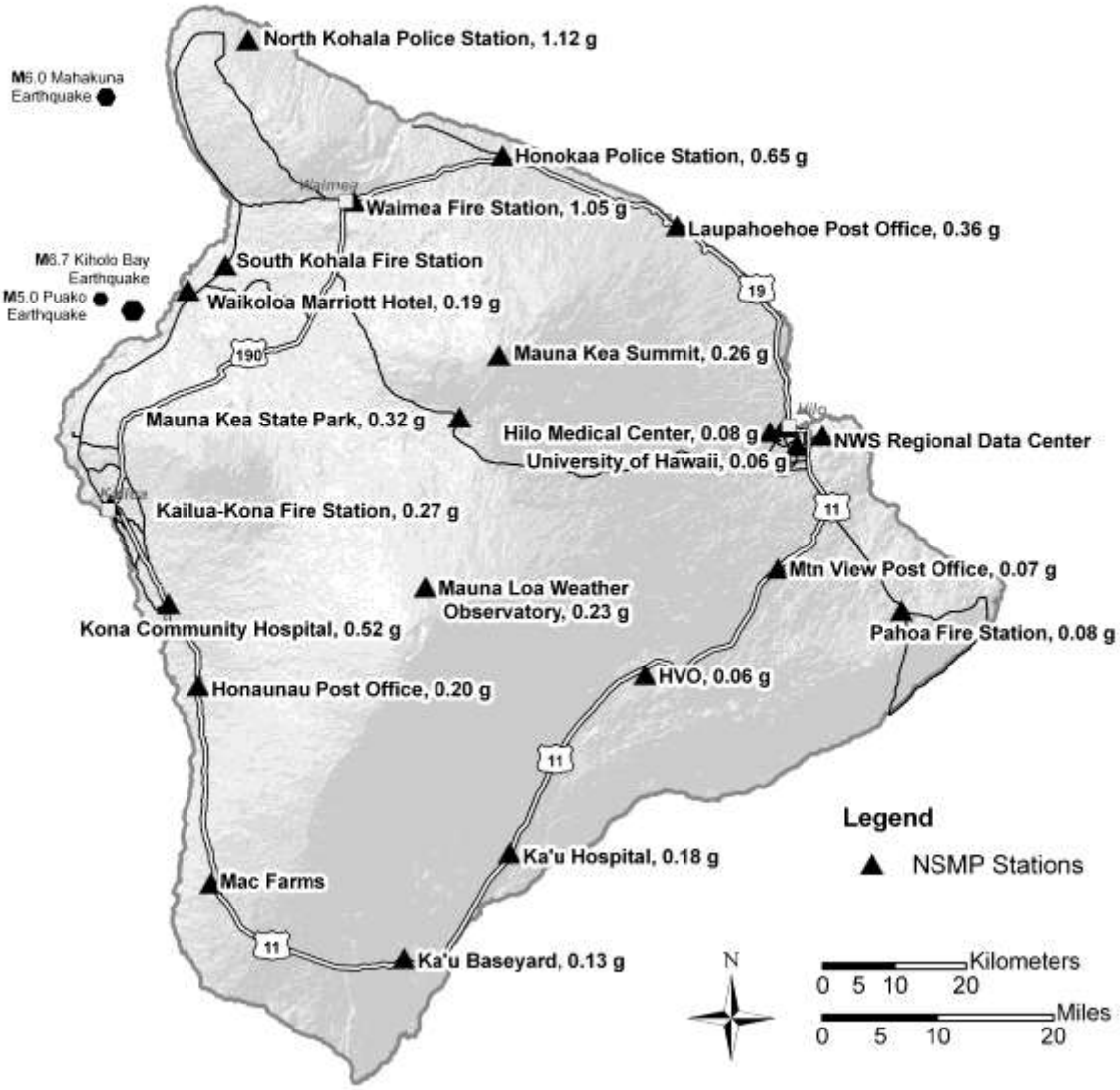
North Kohala Police Station, 1.12 g
M6.0 Mahakuna Earthquake
Honokaa Police Station, 0.65 g
Waimea
Waimea Fire Station, 1.05 g
Laupahoehoe Post Office, 0.36 g
M6.7 Kiholo Bay Earthquake
South Kohala Fire Station
M5.0 Puako Earthquake
Waikoloa Marriott Hotel, 0.19 g
19
190
Mauna Kea Summit, 0.26 g
Mauna Kea State Park, 0.32 g
Hilo
Hilo Medical Center, 0.08 g
NWS Regional Data Center
University of Hawaii, 0.06 g
Kailua
Kailua-Kona Fire Station, 0.27 g
11
Mtn View Post Office, 0.07 g
Mauna Loa Weather Observatory, 0.23 g
Kona Community Hospital, 0.52 g
Pahoa Fire Station, 0.08 g
HVO, 0.06 g
Honaunau Post Office, 0.20 g
11
Legend
NSMP Stations
Ka'u Hospital, 0.18 g
Mac Farms
11
Ka'u Baseyard, 0.13 g
N
Kilometers
0 5 10 20
Miles
0 5 10 20

Figure 1

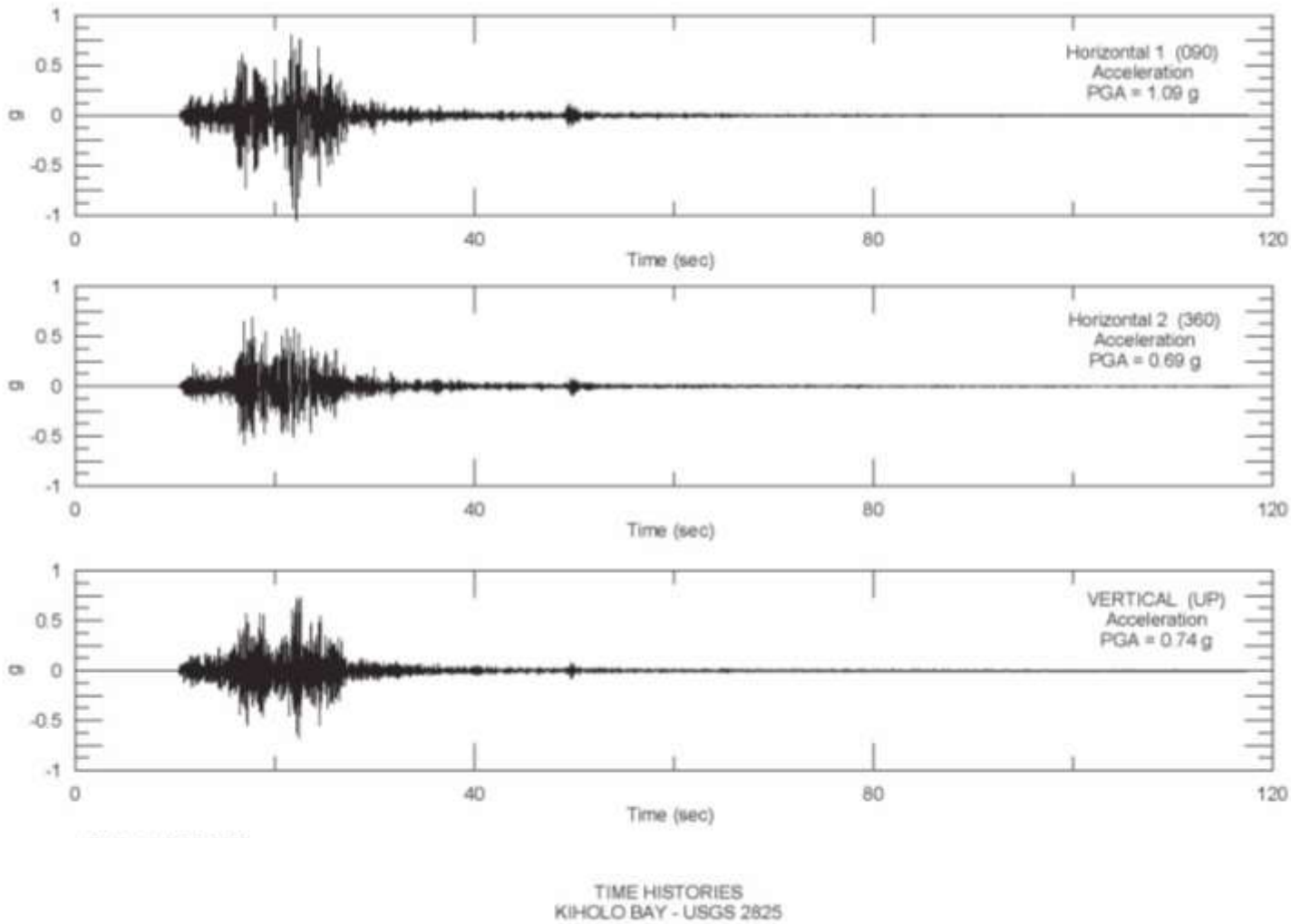
Horizontal 1 (090)
Acceleration
PGA = 1.09 g
Horizontal 2 (360)
Acceleration
PGA = 0.69 g
VERTICAL (UP)
Acceleration
PGA = 0.74 g
g
Time (sec)
TIME HISTORIES
KIHOLO BAY - USGS 2825

Figure 2

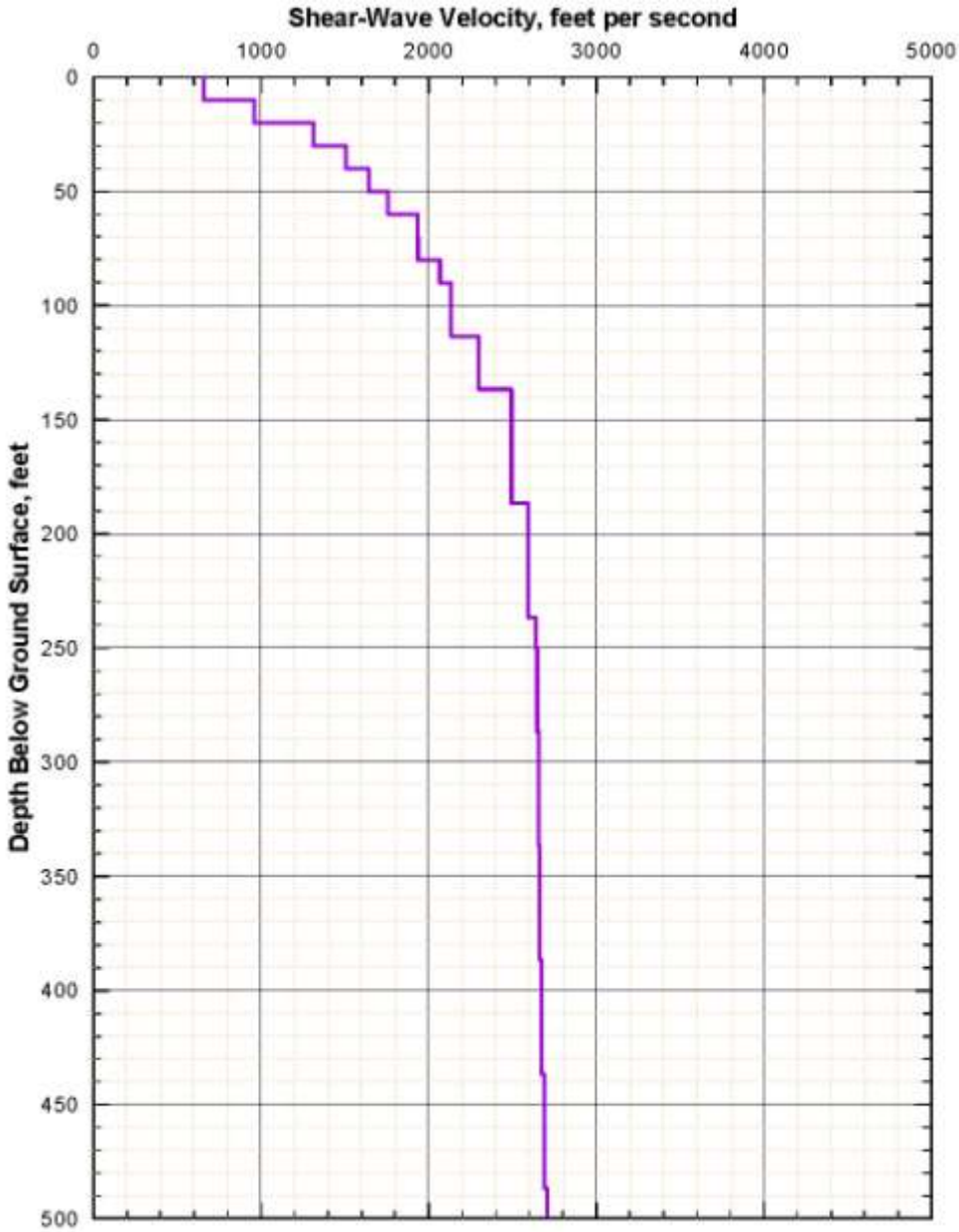
Shear-Wave Velocity, feet per second
0
1000
2000
3000
4000
5000
Depth Below Ground Surface, feet
0
50
100
150
200
250
300
350
400
450
500

Figure 3

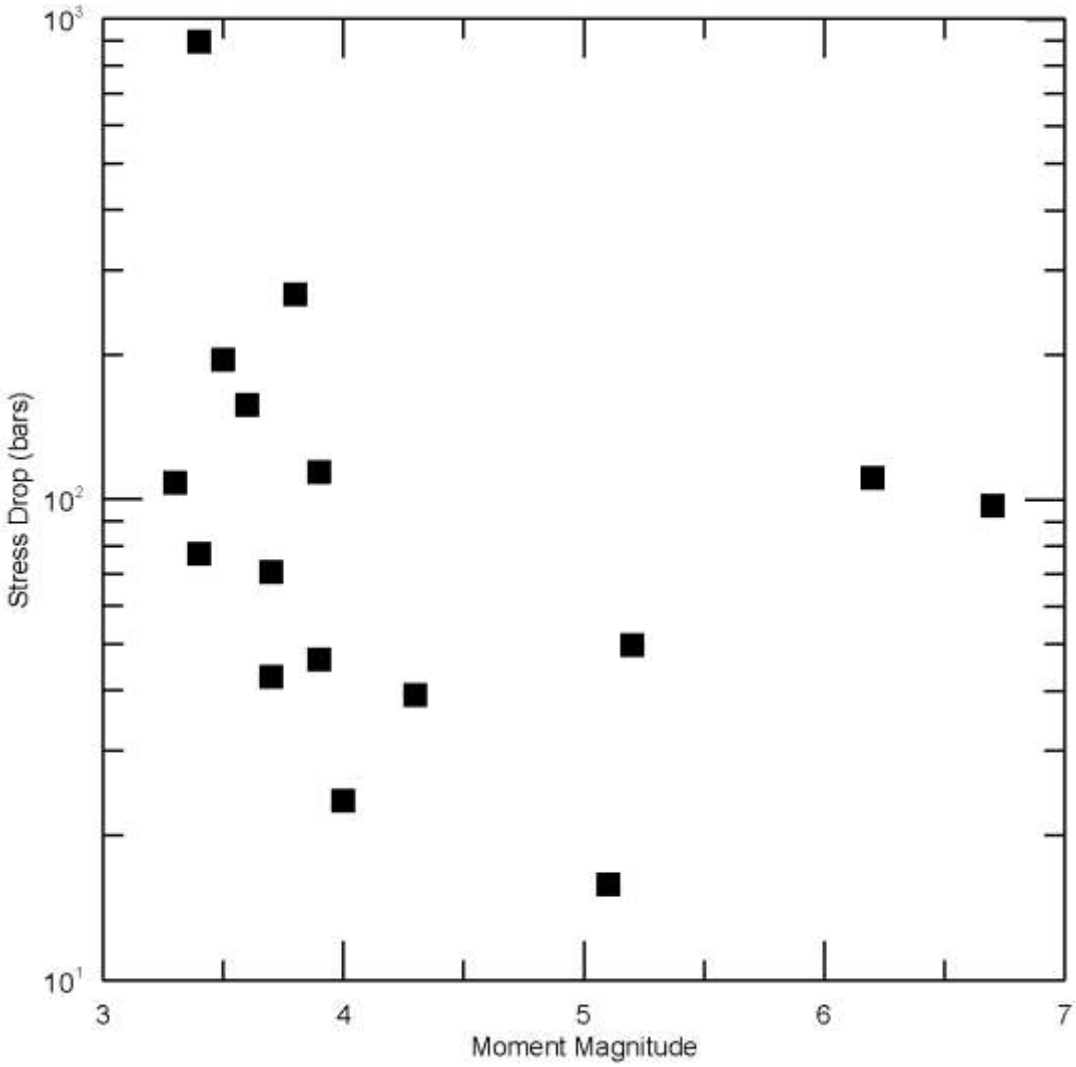

Figure 4

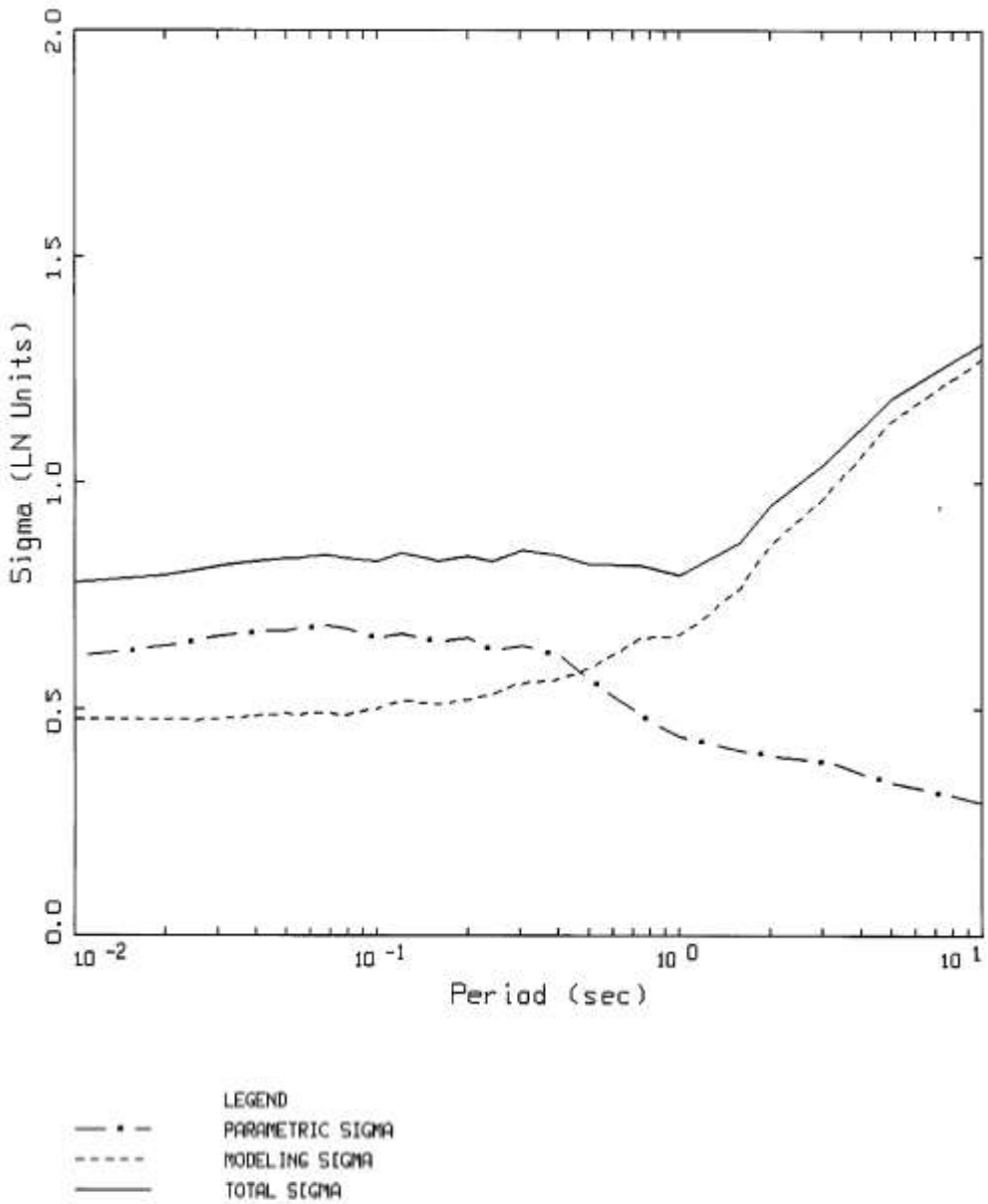
2.0
1.5
1.0
0.5
0.0
Sigma (LN Units)
10 -2
10 -1
10 0
10 1
Period (sec)
LEGEND
PARAMETRIC SIGMA
MODELING SIGMA
TOTAL SIGMA

Figure 5

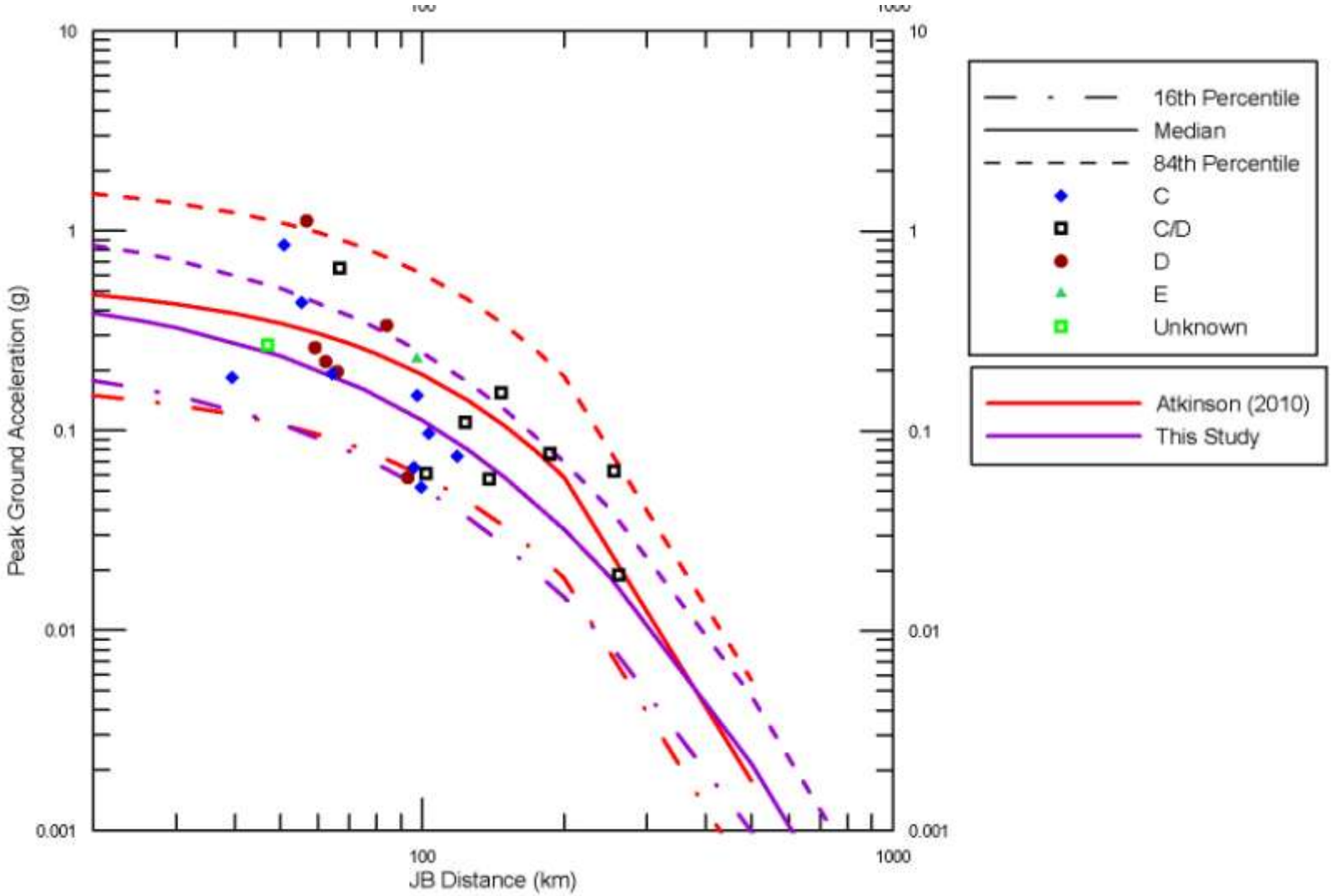
10
1
0.1
0.01
0.001
Peak Ground Acceleration (g)
100
1000
JB Distance (km)
16th Percentile
Median
84th Percentile
C
C/D
D
E
Unknown
Atkinson (2010)
This Study

Figure 6

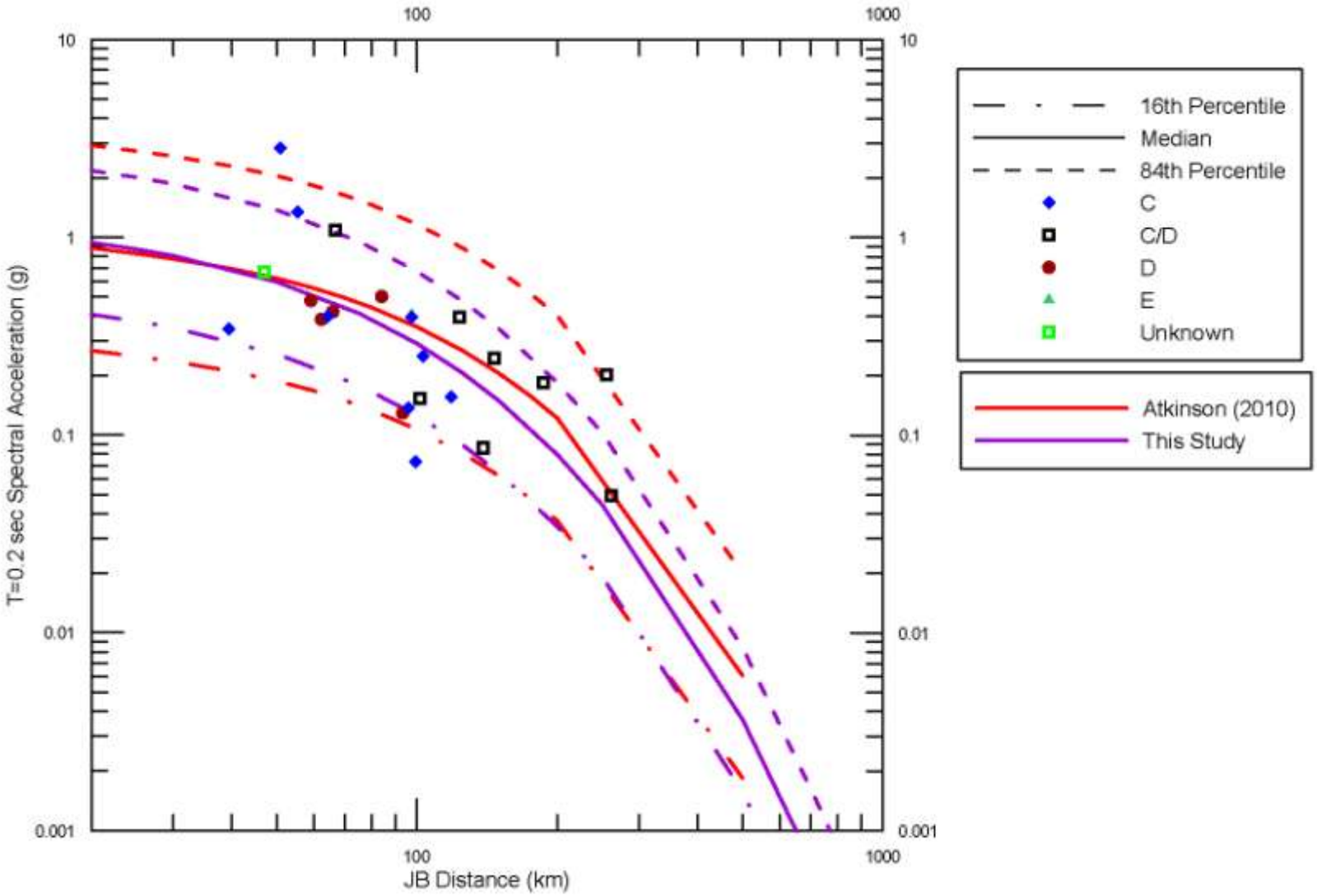
100
1000
10
1
0.1
0.01
0.001
T=0.2 sec Spectral Acceleration (g)
JB Distance (km)
16th Percentile
Median
84th Percentile
C
C/D
D
E
Unknown
Atkinson (2010)
This Study

Figure 7

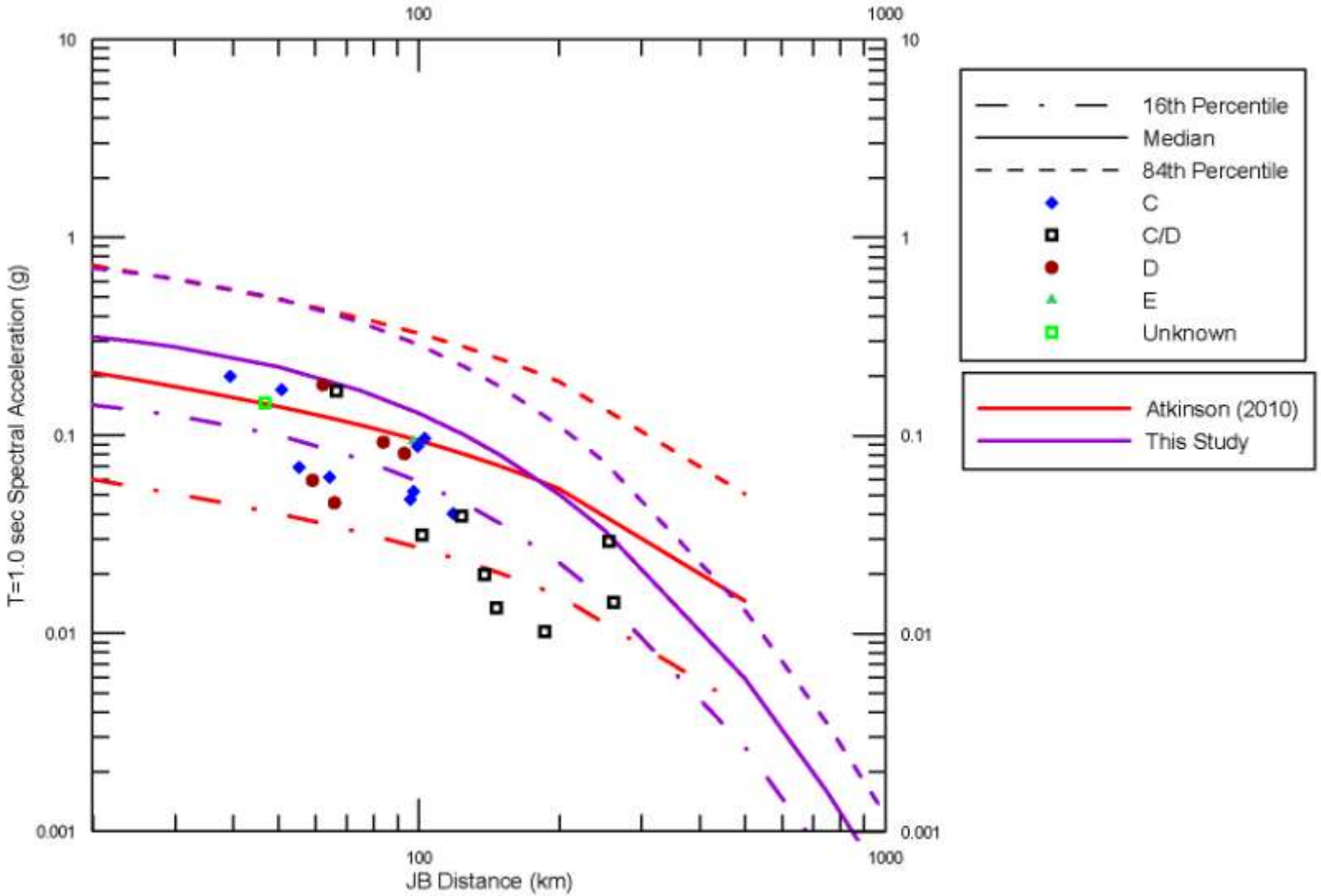
100
1000
10
1
0.1
0.01
0.001
T=1.0 sec Spectral Acceleration (g)
JB Distance (km)
16th Percentile
Median
84th Percentile
C
C/D
D
E
Unknown
Atkinson (2010)
This Study

Figure 8

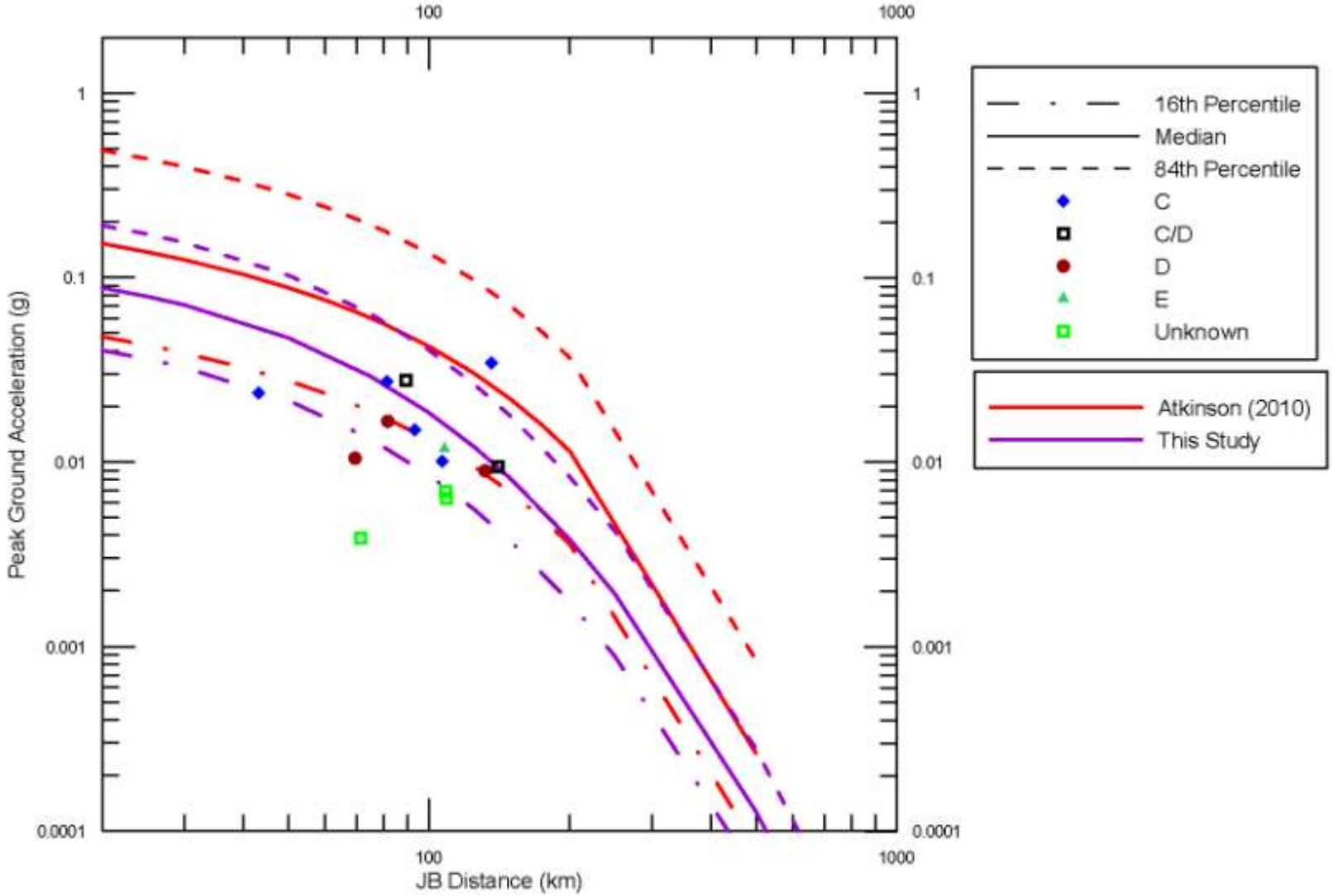
100
1000
1
0.1
0.01
0.001
0.0001
Peak Ground Acceleration (g)
JB Distance (km)
16th Percentile
Median
84th Percentile
C
C/D
D
E
Unknown
Atkinson (2010)
This Study

Figure 9

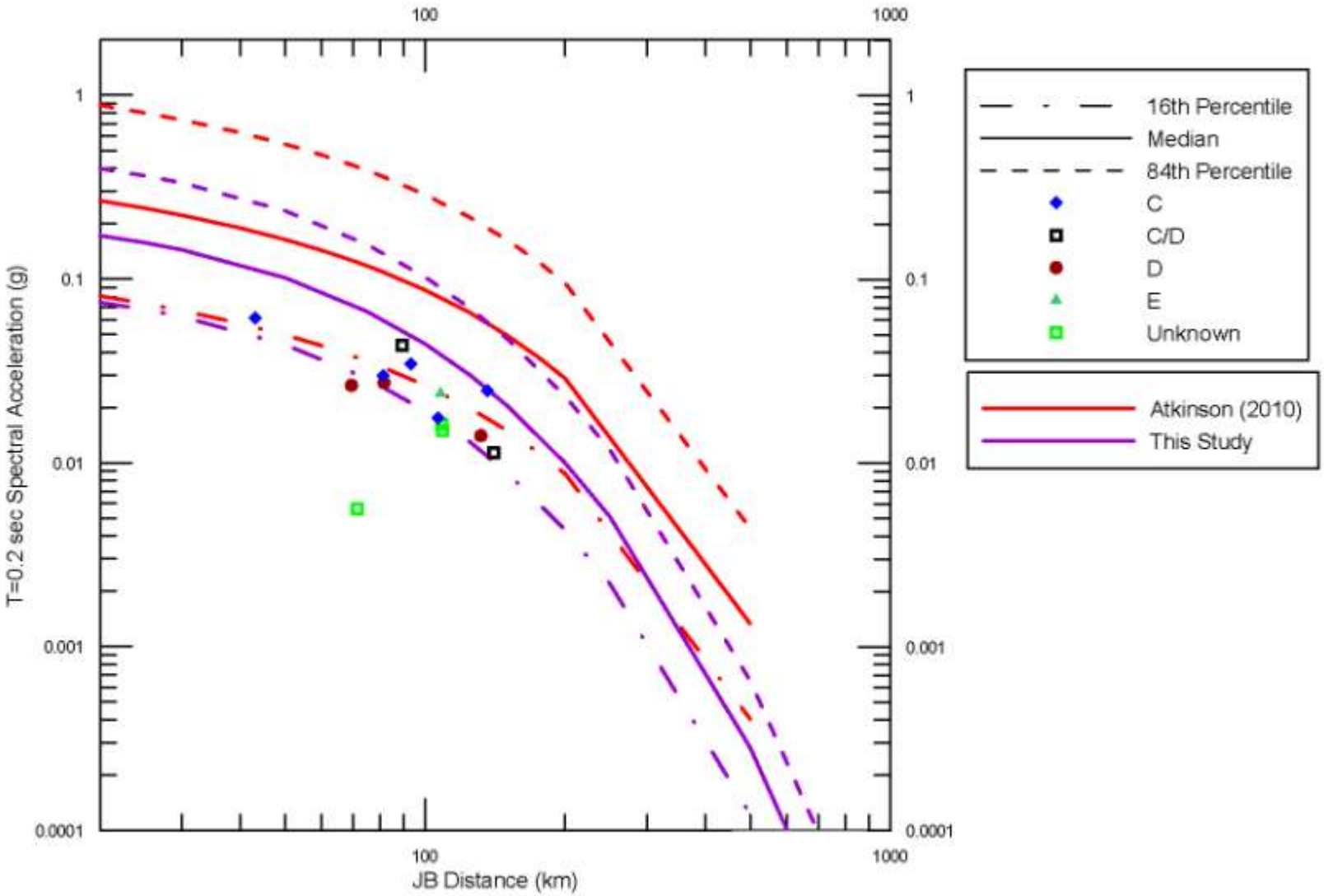
100
1000
1
0.1
0.01
0.001
0.0001
T=0.2 sec Spectral Acceleration (g)
JB Distance (km)
16th Percentile
Median
84th Percentile
C
C/D
D
E
Unknown
Atkinson (2010)
This Study

Figure 10

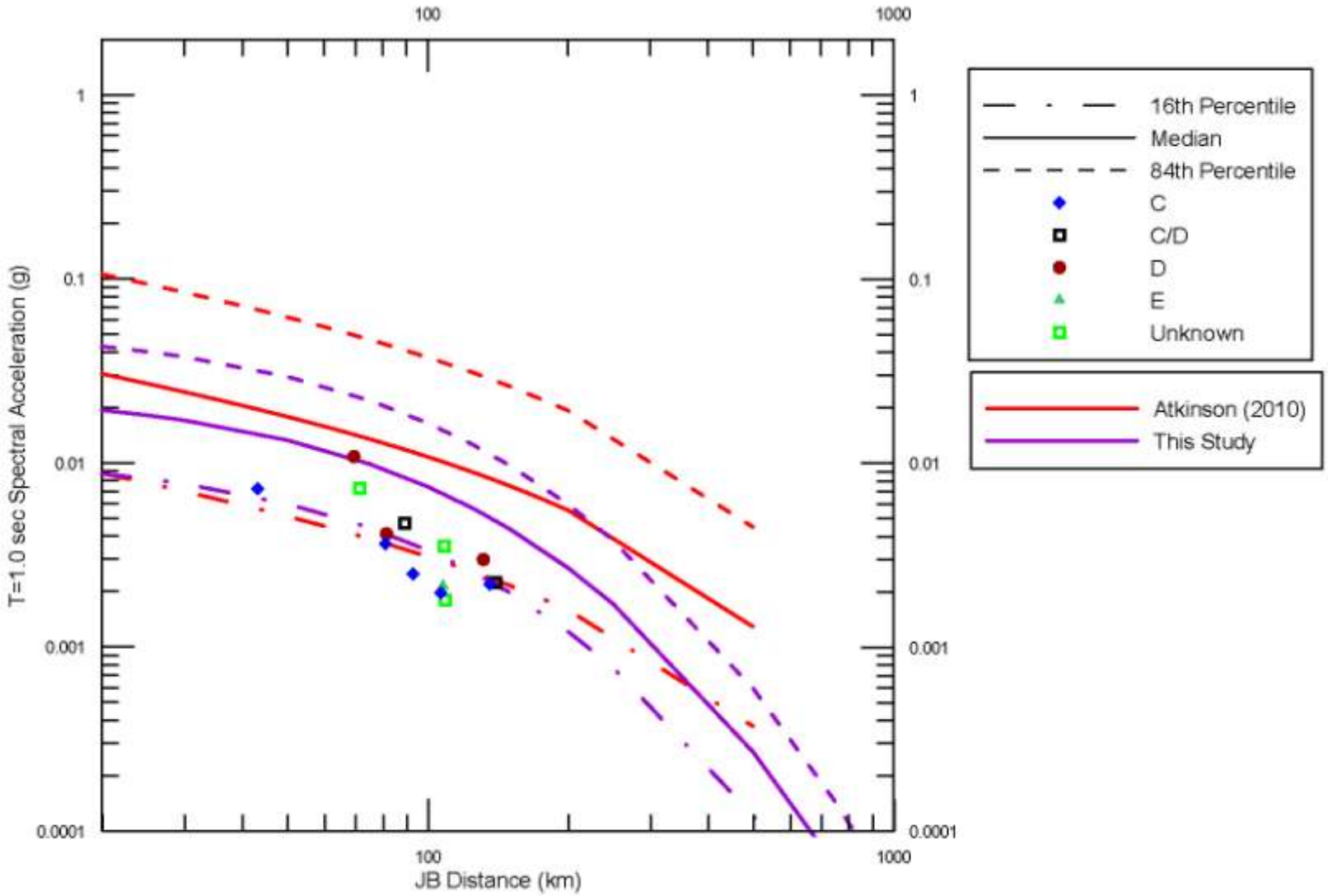
100
1000
1
0.1
0.01
0.001
0.0001
T=1.0 sec Spectral Acceleration (g)
JB Distance (km)
16th Percentile
Median
84th Percentile
C
C/D
D
E
Unknown
Atkinson (2010)
This Study

Figure 11

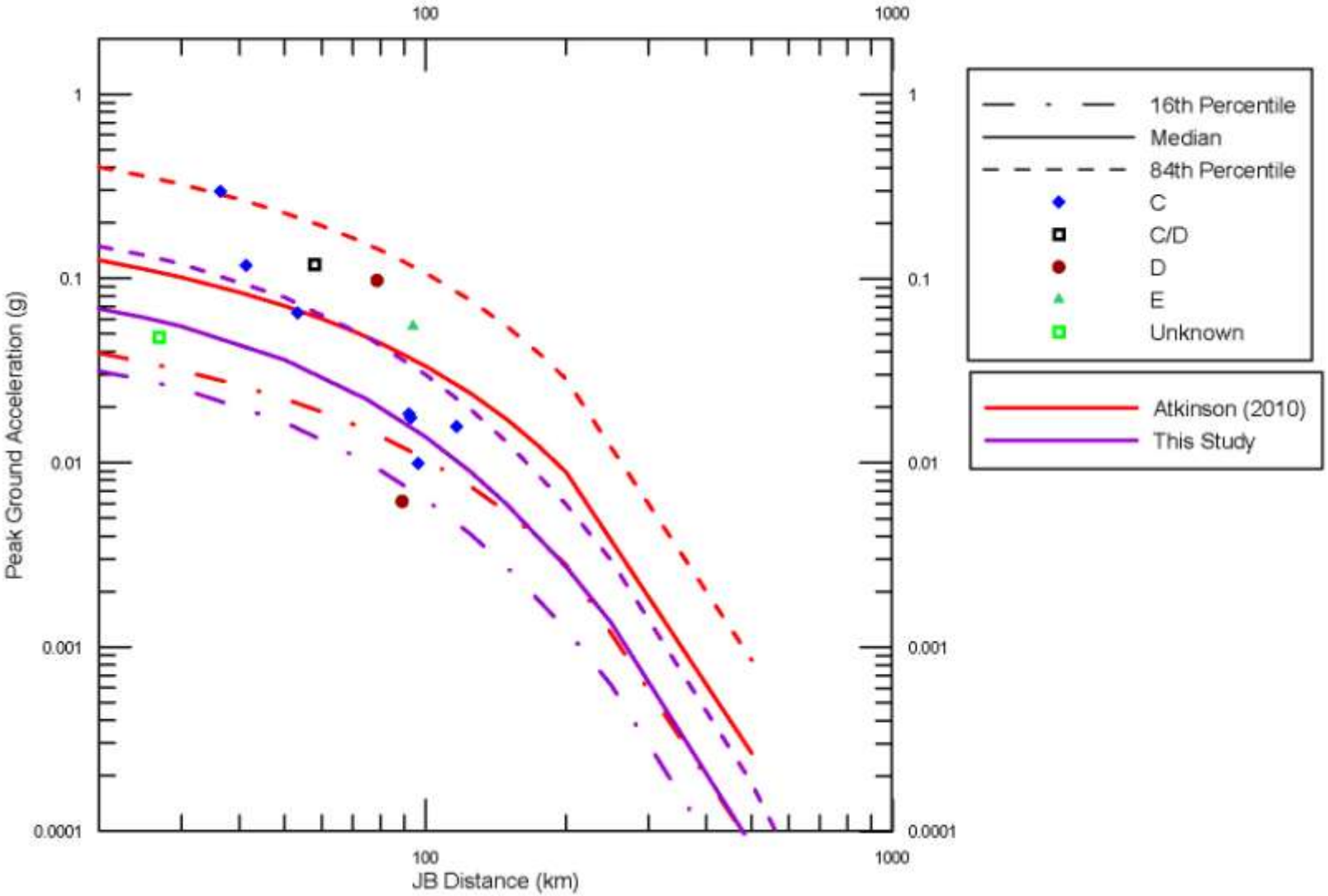
100
1000
1
0.1
0.01
0.001
0.0001
Peak Ground Acceleration (g)
JB Distance (km)
16th Percentile
Median
84th Percentile
C
C/D
D
E
Unknown
Atkinson (2010)
This Study

Figure 12

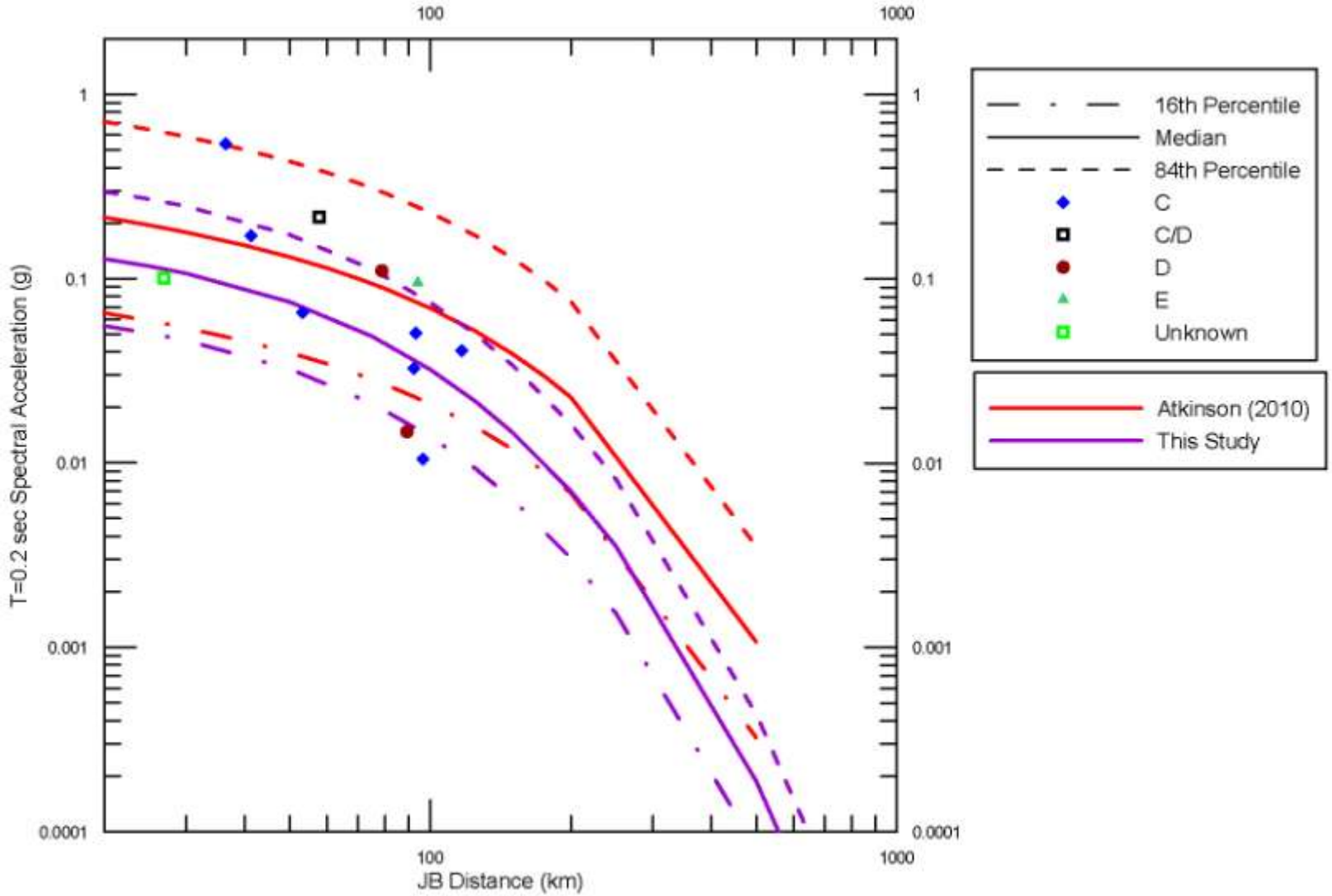
100
1000
1
0.1
0.01
0.001
0.0001
T=0.2 sec Spectral Acceleration (g)
JB Distance (km)
16th Percentile
Median
84th Percentile
C
C/D
D
E
Unknown
Atkinson (2010)
This Study

Figure 13

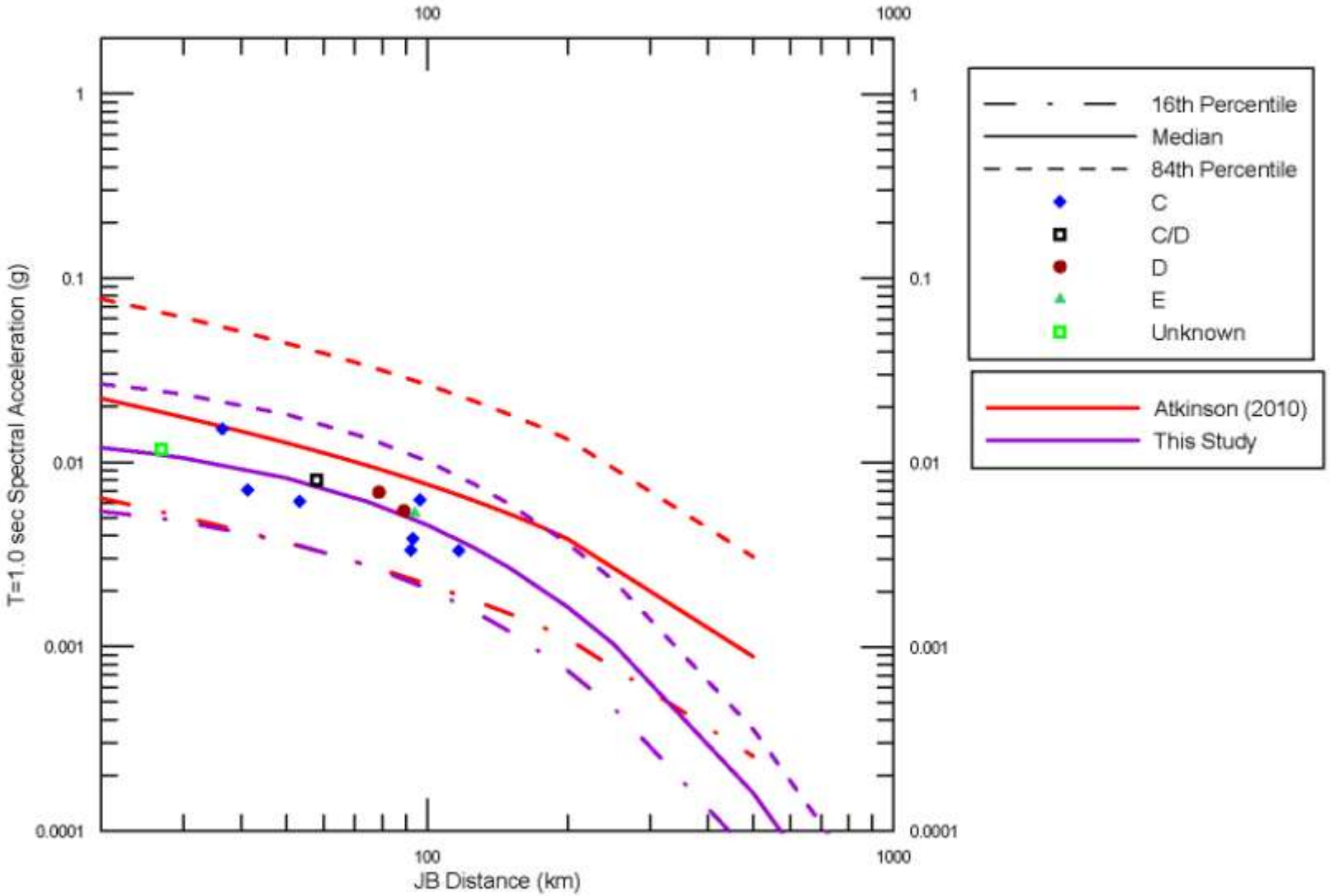
100
1000
1
0.1
0.01
0.001
0.0001
T=1.0 sec Spectral Acceleration (g)
JB Distance (km)
16th Percentile
Median
84th Percentile
C
C/D
D
E
Unknown
Atkinson (2010)
This Study

Figure 14